# Experimental Evaluation of Medium-Voltage Cascode Gallium Nitride (GaN) Devices for Bidirectional DC–DC Converters

Salah S. Alharbi, and Mohammad Matin, *Senior Member, IEEE*

***Abstract*—Wide bandgap (WBG) semiconductors, such as silicon carbide (SiC) and gallium nitride (GaN), exhibit superior physical properties and demonstrate great potential for replacing conventional silicon (Si) semiconductors with WBG technology, pushing the boundaries of power devices to handle higher blocking voltages, switching frequencies, output power levels, and operating temperatures. However, tradeoffs in switching performance and converter efficiency when substituting GaN devices for Si and SiC counterparts are not well-defined, especially in a cascode configuration. Additional research with further detailed investigation and analysis is necessitated for medium-voltage GaN devices in power converter applications. Therefore, the aim of this research is to experimentally investigate the impact of emerging 650/900 V cascode GaN devices on bidirectional dc–dc converters that are suitable for energy storage and distributed renewable energy systems. Dynamic characteristics of Si, SiC, and cascode GaN power devices are examined through the double-pulse test (DPT) circuit at different gate resistance values, device currents, and DC bus voltages. Furthermore, the switching behavior and energy loss as well as the rate of voltage and current changes over the time are studied and analyzed at various operating conditions. A 500 W experimental converter prototype is implemented to validate the benefits of cascode GaN devices on the converter operation and performance. Comprehensive analysis of the power losses and efficiency improvements for Si-based, SiC-based, and GaN-based converters are performed and evaluated as the switching frequency, working temperature, and output power level are in-creased. The experimental results reveal significant improvements in switching performance and energy efficiency from the emerging cascode GaN devices in the bidirectional converters.**

***Index Terms*—Bidirectional dc–dc converters, cascode GaN-FETs, double-pulse test, energy efficiency, power loss analysis, SiC-MOSFET, SiC-Schottky diode, switching characterization.**

Manuscript received June 13, 2020; revised November 07, 2020; accepted November 25, 2020. date of publication September 25, 2021; date of current version September 18, 2021.

The authors would like to thank Transphorm Inc. for providing new cascode GaN-FET device samples and Dr. Wenzhong Gao for his lab and equipment supports. *(Corresponding Author: Salah S. Alharbi)*

Salah S. Alharbi is with an Assistant Professor of Electrical Engineering in the School of Engineering at Albaha University, Alaqiq, in Saudi Arabia (e-mail: ssalharbi@bu.edu.sa, salah.alharbie@gmail.com). Mohammad Matin is with a Professor of Electrical and Computer Engineering in the School of Engineering and Computer Science at University of Denver, Denver, CO, in USA. He is a senior Member of IEEE, OSA, SPIE, and member of ASEE and Sigma Xi.

Digital Object Identifier 10.30941/CESTEMS.2021.000227

## I. Introduction

As renewable energy sources, such as photovoltaic (PV) and wind, are rapidly implemented in DC microgrids, energy storage systems play a significant role in ensuring uninterrupted power supply and in supporting the reliability and stability of microgrid operations [1]–[4]. Power electronics, especially bidirectional dc–dc converters, are essential parts in distributed energy storage and alternative energy systems because of their grid synchronization, DC power management, and bidirectional power flow capabilities [5]–[8]. Among various non-isolated dc–dc bidirectional topologies, buck–boost (half-bridge) converters are widely employed in DC microgrids due to their prominent advantages of increased efficiency, improved reliability, straightforward structure, uncomplicated control system, reduced size, and minimal cost [9]–[11]. However, these bidirectional converters have major disadvantages of a limited voltage conversion ratio between input and output as well as a high voltage stress across switching devices, leading to critical challenges in improving the reliability of the switches and the capability of the converter [12]–[14]. Furthermore, most existing converters are suffering from intensive conduction and switching losses under harsh operating conditions associated with power semiconductor devices, which are essential components of power electronics [15]–[17].

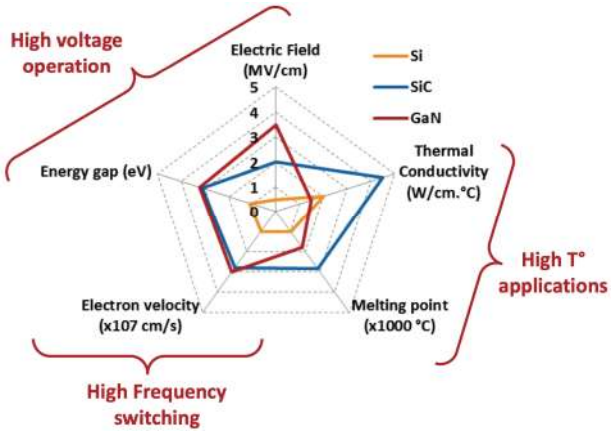


Fig. 1. Key material properties of Si and WBG semiconductors [18].

Traditional silicon (Si) is by far the most commonly used semiconductor material for switching devices. The performance and efficiency of conventional bidirectional dc–dc converters are hindered by Si-based power devices, which are

approaching their theoretical and physical limits [19]–[21]. Consequently, the restrictions of Si power switches are a rigid barrier to obtaining significant improvements in the performance and efficiency of converters based upon this technology. Academic and industrial researchers have devoted significant efforts and numerous resources to develop and fabricate alternative semiconductor materials with improved characteristics for next-generation power devices due to the limitations of Si devices and an acute global demand for power devices with higher operating capabilities [22], [23]. Emerging wide bandgap (WBG) semiconductors, such as gallium nitride (GaN) and silicon carbide (SiC), exhibit superior material properties than traditional Si materials, enabling power devices to operate effectively under harsh operating conditions [24]–[26]. WGB materials offer outstanding physical properties like a wider energy gap, better thermal conductivity, higher electron mobility, higher saturated velocity, and larger critical electric field [27]–[30]. Physical properties of different semiconductor materials are described in Fig 1.

Due to GaN superior physical properties, GaN technology offers the most promising solution among other proposed ones for improving power electronic applications [31]–[35]. Although there is a limited research, like [36]–[39], that evaluated 650 V cascode GaN power devices, most published works, such as [40]–[45], have not comprehensively demonstrated the switch-ing behavior of these devices at the medium-voltage level, above than 650 V. These works show inconsistent voltage level and device package, which play an important role in converter efficiency and performance due to different parasitic elements and gate circuit suitability. Therefore, further investigations on 900/650 V cascode GaN-FETs used in power converters are needed to better understand the switching behavior of these new devices and compared with existing Si and SiC devices at the same voltage rate within the same device package. Additionally, none of the aforementioned published research provides the necessary information and practical data to support using 900 V cascode GaN-FET devices integrated into power converters. Although cascode GaN-FET devices were studied by some re-searchers [46]–[48], the tradeoffs in the switching performance, efficiency, size, and cost of the GaN-based converters are still unclear in the literature, especially at 900 V.

This research attempts to close this knowledge gap by comprehensively studying and evaluating 900 V GaN-FET devices integrated into the bidirectional dc–dc converters. To facilitate this important research, Transphorm provided a sample of new 900 V cascode GaN-FET (TP90H050WS) in the TO-247 package. This device is not yet commercially available, but it is expected to be released before the end of 2020. The motivation for this research is to provide the essential information and practical tools for incorporating cascode GaN-FET devices into power converters. It includes a detailed dynamic characterization of GaN-FET devices and compares their switching behavior to Si and SiC counterparts as well as evaluates experimentally the GaN-based converter performance under harsh operating conditions.

This paper is organized in the following manner. Section II describes the bidirectional converter topology and converter operation with design specifications. Section III illustrates GaN semiconductor technology with different power devices used in the power converter. Section IV presents the switching characterization methodology with experimental set-up and analyzes their power losses. Section V investigates switching behavior of power devices during the turn-on and turn-off transitions. Section VI assesses the switching energy loss of each power device at different operating conditions. Section VII evaluates overall converter performance with different power device combinations to identify total power loss and energy efficiency at high operating conditions. Section VIII presents the cost of various power devices integrated into the bidirectional converters. Finally, section IX summarizes the research findings.

## II. BIDIRECTIONAL DC–DC TOPOLOGY

Bidirectional converters play a pivotal role in interfacing DC microgrid, including various distributed energy systems, with utility network and they control power flow and microgrid operation during the grid-connected mode and islanding mode [49]. These converters are indispensable parts in automotive systems and energy storage devices to provide different voltage ratios between input and output sides along with improving the power conversion system and the stability of the DC microgrid [50]. Fig. 2 depicts a typical DC microgrid where bidirectional power electronics are vastly implemented. Based on the galvanic isolation between the input and output voltages [51], bidirectional dc–dc converters are classified into two major groups of configurations which are isolated and non-isolated converters.

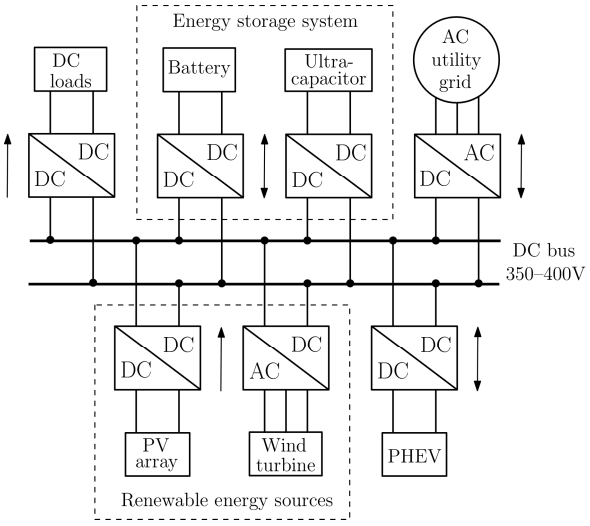


Fig. 2. A typical DC microgrid system where various bidirectional converters considerably used.

### A. Non-Isolated Bidirectional dc-dc Converter

Non-isolated, which is known as transformer-less, bidirectional dc–dc converters are increasingly gaining a lot of attention due to the acute need to power electronics with high efficiency and bidirectional power flow capability between two DC buses or energy storage sources. Because these converters do not implement electrical galvanic isolation in their

configuration, they outstandingly exhibit appealing advantages of straightforward structure, light weight, increased efficiency, improved power density, and reduced size as well as minimized cost. Fig. 3 depicts the schematic of the non-isolated bidirectional (half-bridge) buck-boost converter, which is connecting a low-side voltage ($V_L$), such as a battery or super-capacitor, with a high-side voltage ($V_H$ ), like DC link or bus. This converter is composed of one inductor ($L$), two capacitors ($C_1$, $C_2$) for low-side and high-side voltages, two switching devices ($S_1$, $S_2$), and two anti-parallel diodes ($D_1$, $D_2$), acting as free-wheeling diodes.

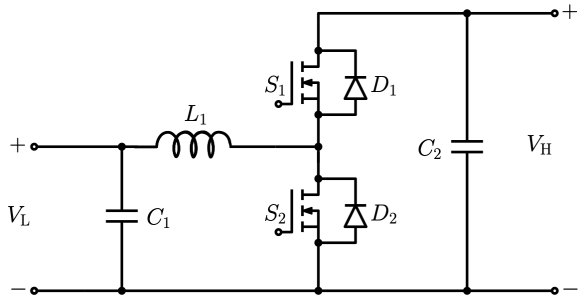


Fig. 3. Non-isolated bidirectional dc–dc buck-boost converter structure.

### B. Converter Operation and Modeling

The bidirectional converter performs as a buck converter (discharge mode) from the low voltage to high voltage and it works as a boost converter (charge mode) when operating in the reverse direction. In the bidirectional dc–dc buck-boost converter, the inductor is considered the main energy transfer element, which is accountable for the output current ripple. This converter can step-down or step-up the voltage depending on the status of two power switching devices, such as MOSFETs and IGBTs, combined with anti-parallel diodes, which are acting as freewheeling diodes, respectively.

Furthermore, the state-space averaging approach is applied for the modeling of the bidirectional dc–dc buck-boost converter with balanced current and small ripple assumptions as well as the dead-time effect and the variation of conduction voltage drop in bidirectional power flow directions are neglected. It is noteworthy that the inductor parasitic resistance ($R_{lp}$) and on-state resistance ($R_{ds(\text{on})}$) are involved in this model because they exhibit a critical impact on converter performance. The converter can operate either charge or discharge mode while each mode has always two intervals. In the buck mode, when the $S_1$ switch is turned on and the $S_2$ switch is turned off, the voltage across inductor and two capacitors are illustrated, as follows:

$$L\frac{di_L}{dt}+di_L\left(R_{lp}-R_{ds(on)}\right)=v_{c2}-v_{c1} \tag{1}$$

$$C_1\frac{dv_{c1}}{dt}=i_L-\frac{v_{c1}-V_L}{R_L} \tag{2}$$

$$C_2\frac{dv_{c2}}{dt}=-\left(i_L-\frac{v_{c2}-V_H}{R_L}\right) \tag{3}$$

where $\Delta i_L$ and $\Delta$vc are the inductor ripple current and capacitor ripple voltage. $v_{c1}$ and $v_{c2}$ are low-side and high-side capacitor voltages while $R_L$ and $R_H$ are low-side and high-side resistive loads. In the boost mode, when the $S_2$ switch is turned on and the $S_1$ switch is turned off, the voltage across inductor and two capacitors are described, as follows:

$$L\frac{di_L}{dt}+di_L\left(R_{lp}-R_{ds(on)}\right)=-v_{c1} \tag{4}$$

$$C_1\frac{dv_{c1}}{dt}=i_L-\frac{v_{c1}-V_L}{R_H} \tag{5}$$

$$C_2\frac{dv_{c2}}{dt}=-\frac{v_{c2}-V_H}{R_L} \tag{6}$$

### C. Converter Design and Consideration

Table I highlights the converter specifications, which are compatible with renewable energy sources and energy storage applications employed in DC microgrid system. The converter is designed to operate in continuous conduction mode (CCM) in order to investigate the impacts of different power devices on overall converter performance. The size of reactive components, such as capacitors and inductors, is characterized based on their optimal values and determined in the buck-mode and boost-mode operation, taking different switching frequencies into consideration.

TABLE I
DESIGN SPECIFICATIONS FOR THE BIDIRECTIONAL DC-DC CONVERTER.

| Converter parameter | Symbol | Value |
|---|---|---|
| Rating power | $P_r$ | 500 W |
| High-side (DC bus) voltage | $V_H$ | 400 V |
| Low-side (Battery) voltage | $V_L$ | 48-96 V |
| Switching frequency | $f_{sw}$ | 40-200 kHz |
| Inductor | $L$ | 20 mH |
| Low-side and high-side capacitors | $C_1, C_2$ | 16 μF |

## III. GALLIUM NITRIDE POWER DEVICES

GaN power devices are gaining considerable attention for next-generation power electronic converters because these de-vices exhibit physical properties superior to those of traditional Si materials, providing great potential for power conversion systems. As semiconductor switching devices are the main elements of power converters, it is important to understand their switching characteristics and performance in order to employ cascode GaN devices in converter designs.

### A. Cascode GaN Technology

Based on different structures of the gate terminal, GaN heterojunction field effect transistors (HFETs) can be fabricated and constructed in depletion-mode or enhancement-mode, which is determined by the internal material structure and layout during the production process [52], [53]. Fig. 4 shows different modes of GaN devices, which are depletion-mode and enhancement-mode [54]. The depletion-mode of GaN HEMTs is normally-on so it can be difficult to incorporate these devices into high-power conversi-

TABLE II
KEY PARAMETERS OF POWER DEVICES INTEGRATED INTO BIDIRECTIONAL CONVERTERS.

| Device | Transphorm | Cree | Infineon | Cree | Infineon |
|---|---|---|---|---|---|
| Semiconductor technology | Cascode GaN-FET TP90H050WS | SiC-MOSFET C3M0065090D | Si-MOSFET IPW90R120C3 | SiC-Schottky diode C3D16065D1 | Si-diode IDW30C65D1 |
| $V_{ds}$ | 900 V | 900 V | 900 V | 650 V | 650 V |
| $V_{gs}$ | ±20 V | -8/+19 V | ±30 V | N/A | N/A |
| $I_d$ (@ 25℃) | 34 A | 36 A | 36 A | 43 A | 30 A |
| $R_{ds}$(on)(@ 25℃) | 50 mΩ | 65 mΩ | 100 mΩ | N/A | N/A |
| $T_j$ (max) | 150℃ | 150℃ | 150℃ | 150℃ | 175℃ |
| $V_f$(@ 25℃) | N/A | N/A | N/A | 1.5 V | 1.7V |
| Package | TO-247 | TO-247 | TO-247 | TO-247 | TO-247 |

on systems where normally-off switches are more suitable due to operational safety considerations and gate-driver circuitry simplicity. However, the cascode structure, which is basically adding another transistor in a series way, overcomes this issue, resulting in a normally-off device. Though this structure has the disadvantage of increasing on-state resistance, this issue becomes insignificant at high-voltage levels since the on-resistance of the high-voltage GaN device is not greatly affected through combining a low-voltage Si transistor into the device.

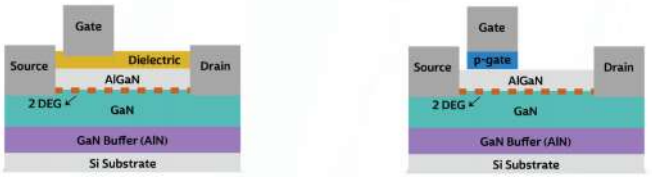


Fig. 4. The cascode depletion-mode (left) and enhancement-mode (right) of GaN power devices [54].

The cascode GaN-FET consists of a low-voltage normally-off Si-MOSFET and a high-voltage normally-on GaN-HEMT in series configuration. The cascode GaN device structure is illustrated in Fig. 5. The combination of Si-MOSFET and GaN-HEMT is packaged in a cascode configuration and it acts as one single transistor, which is called a cascode GaN-FET device. The two switching devices are linked together so that the output drain-source voltage of the Si-MOSFET controls the input gate-source voltage of the GaN-HEMT. In this package, the current flows through the Si-MOSFET and GaN-HEMT during the on-state event while the blocking voltage is shared between the two devices during the off-state event. The main advantages of cascode GaN-FETs are very low reverse recovery charge and gate charge along with a small crossover loss. Among others GaN switches, these devices are more robust and reliable in terms of a wide gate safety margin, high-transient over-voltage capability, and intrinsic lifetime test. Operationally, cascode GaN-FETs offer increased safety and gate-driver circuitry simplicity along with lower ringing behavior of the switching device.

### B. *Different Power Device Selection*

The electrical characteristic and switching behavior of power devices play a significant role in the conversion system since semiconductor switching devices are core element in the power converters. GaN and SiC power devices are the most mature WBG semiconductors and they are well-established and commercially available. These devices a withstand high

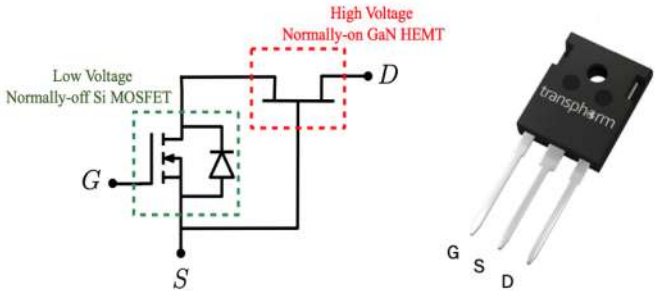


Fig. 5. A high voltage normally-on GaN HEMT with a low voltage normally-off Si MOSFET in a cascode configuration [54].

operating temperatures and switching frequencies, allowing for smaller cooling systems and passive components. They also exhibit lower on-state resistance, leading to reduce conduction loss. In order to investigate the impact of different semiconductor switching devices on the converter level, cascode GaN-FET, Si-MOSFET, and SiC-MOSFET are integrated individually into the power converter to compare and assess their performance in terms of switching behavior and energy efficiency.

Table II provides the key parameters of each semiconductor device employed in the converter performance comparison. The aforementioned power devices are chosen based on their similarity in electrical specifications and compatibility with the designed converter. The methodology that adopted for here is to have an equal comparison between different device technologies. This can be obtained by selecting the identical voltage rate and device package as well as the same on-state resistance and current rate for each device if it is possible.

## IV. SWITCHING CHARACTERIZATION METHODOLOGY

### A. *Double-Pulse Test Circuit*

A double-pulse test (DPT) circuit is a very essential step to characterize the switching behavior of various power devices; therefore, this circuit is implemented to evaluate the switching performance during turn-on and turn-off transitions as well as determine the optimal gate requirements for each device. The DPT board is built with DC bus capacitor utilizing a very small equivalent series inductance (ESL), which is 20 nH. The printed circuit board (PCB) traces are designed to contain a low parasitic series inductance for the current path because minimizing the stray inductance, which is 60 nH, can clearly help to decrease the oscillation of switching waveforms for

power devices. This represents the measured data accurately at the device under test (DUT) with reducing testing circuit distortions. Fig. 6 simplifies the built DPT circuit for the switching performance evaluation. The turn-on and turn-off energy losses of each power device are obtained through the DPT circuit. The double-pulse signal is generated from the DC dual-channel function generator (Keysight 33500B) to apply to the gate driver (Infineon 1EDI60I12AH) for the controlling and turning on/off the device. The width of each pulse plays an important role in controlling the current flowing in the inductive load. Thus, the width and magnitude of first and second pulses should be set up very carefully in order to reach to the desired value of device current.

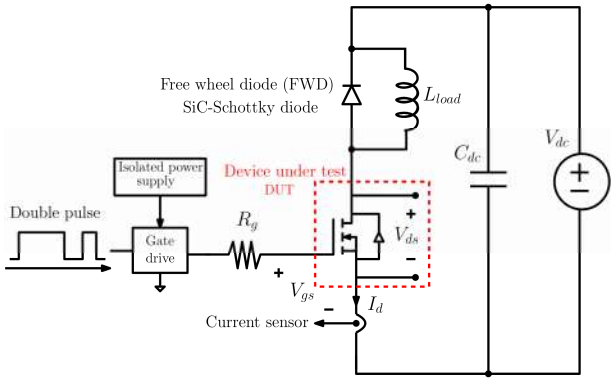


Fig. 6. The schematic of DPT circuit for switching evaluation.

Fig. 7 shows the expected waveforms of drain-source voltage, gate-source voltage, gate under the double-pulse operation during the turn-off and turn-on transitions. These waveforms are captured by a 4-channl digital oscilloscope (Tektronix DPO3014) to obtain waveform data and switching characteristics. In the meantime, the high-voltage differential probes (Tektronix P5200A) are used to measure the drain-source voltage and gate-source voltages as the current sensor (Pearson 2877) is utilized to measure the current passing through the power device. As the device is conducting, the inductor current is increased linearly as shown in Fig. 7. This current is reached to the set-up current value once the device is turned-on at the end of the first pulse by applying negative gate-source voltage. In the switching investigation, the turn-off behavior and energy loss of each device are specified at the end of the first pulse while the turn-on behavior and energy loss of each device are identified at the beginning of the second pulse.

### *B. Equipment and Instruments of DPT Set-up*

The DPT components are presented to examine switching behavior of different power devices and compared their performance at different operating conditions. Table III addresses the main equipment and instruments of DPT circuit that are used for evaluating the switching characterization of each device. Due to virtually zero reverse-recovery effects, the SiC-Schottky diode (C3D16065D1) is utilized in the DPT circuit to offer a freewheeling path for the inductor current as well as to enhance the switching behavior of the two power devices during the turn-on and turn-off transitions. The three tested semiconductor devices, which are Si-MOSFET, SiC-MOSFET, and cascode GaN-FET, are individually assessed through the DPT circuit with the implemented SiC-Schottky diode. Fig. 8 shows the experimental DPT hardware with test instruments, circuit components, and DC power supplies.

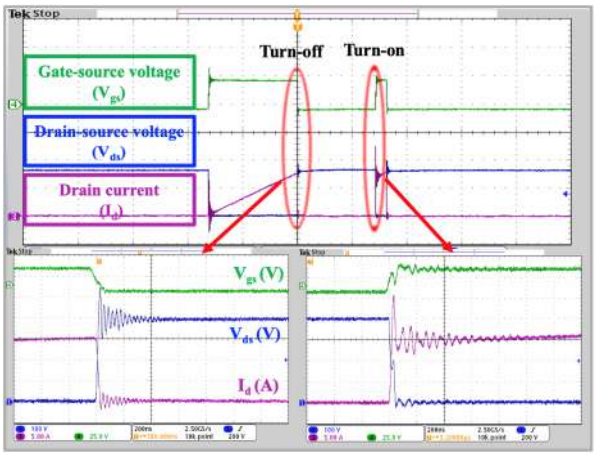


Fig. 7. Drain-source voltage, gate-source voltage, and drain current wave forms under the double-pulse operation during the turn-off and turn-on transitions.

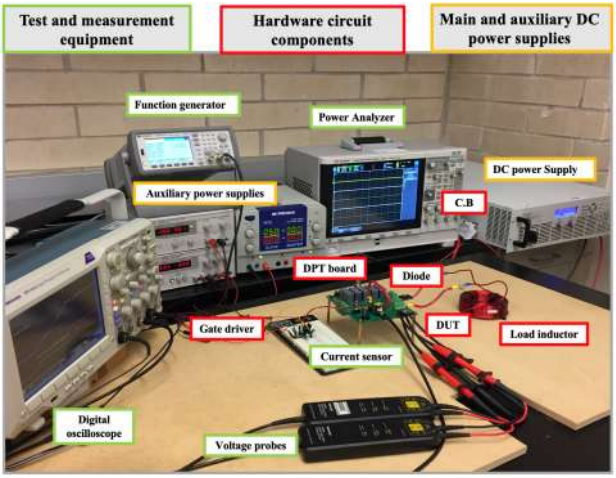


Fig. 8. The experimental DPT circuit.

TABLE III
KEY EQUIPMENT AND INSTRUMENTS FOR THE DPT CIRCUIT.

| Component | Type/value | Deskew |
|---|---|---|
| DC-power supply (N8937A) | 15 kW | - |
| Function generator (33500B) | 30 MHz, 2 channels | - |
| Inductive load (Air core) | 450 μH | - |
| DC capacitor (R75PR4100AA30K) | 20 μF | - |
| Digital oscilloscope (DPO3014) | 100 MHz, 4 channels | - |
| Voltage-differential probe (P5200A) | 50 MHz, 50X/500X | 11.6 ns |
| Pearson current sensor (2878) | 1 Volt/Ampere +1/-0% | 0 ns |
| Digital hot-plate magnetic (MS300) | up to 300℃ | - |

### *C. Semiconductor Power Loss Analysis*

The power dissipation occurred in semiconductor switching devices is important to be analyzed to evaluate the converter performance and efficiency at different operating conditions. Switching devices are generally responsible for the largest

power loss because these devices are major elements in power converters. The main power consumption in semiconductor devices can be divided into conduction and switching losses.

Conduction loss ($P_{con}$) is occurred when the current is flowing through the power device. This loss depends on the static on-state resistance and current of devices. Thus, the conduction loss for power devices such as Si-MOSFET, SiC-MOSFET, and cascode GaN-FET, is expressed as

$$P_{con} = I_{rms}^2 R_{ds(on)} \tag{7}$$

$$P_{con} = V_f I_{avg} + I_{rms}^2 r_{on} \tag{8}$$

where $V_f$ , $I_{avg}$, Irms, and $r_{on}$ are the forward voltage drop, average and room-mean-square values of the device current, and dynamic on-state resistance of the power device, respectively. From Table II, the conduction loss for Si-MOSFET, SiC-MOSFET, and cascode GaN-FET is calculated at different switch currents. Table IV shows a comparison of the conduction loss for these devices at a switching frequency of 50 kHz as the switch current is increased from 4 to 12 A. Clearly, cascode GaN-FET offers a significantly lower conductions loss among different power devices due to its smaller on-state resistance. Fig. 9 shows that conduction loss of all devices is evaluated at two junction temperatures ($T_j$) of 25 and 125℃ while the switching frequency is 50 kHz. It noticed that conduction loss for Si-MOSFET is drastically increased at higher junction temperature while conduction loss for SiC-MOSFET and cascode GaN-FET is increased slightly because WBG devices feature considerably larger electric field and higher thermal conductivity compared to Si devices.

TABLE IV
CONDUCTION LOSS OF DIFFERENT POWER DEVICES.

| Switch current (A) | Conduction loss (W) Si MOSFET | SiC MOSFET | Cascode GaN-FET |
|---|---|---|---|
| 4 | 1.9 | 1.1 | 0.8 |
| 6 | 4.3 | 2.3 | 1.6 |
| 8 | 7.7 | 4.2 | 3.2 |
| 10 | 12 | 6.5 | 5.0 |
| 12 | 17.3 | 9.4 | 7.2 |

Switching loss virtually contributes to a large amount of the total power loss in energy conversion systems. Therefore, this loss is very important to be computed in this section in order to investigate the impact of using Si-MOSFET, SiC-MOSFET, and cascode GaN-FET devices. The switching energy loss for different semiconductor devices used in power converters is obtained and assessed and through the DPT circuit at various operating conditions. Energy loss is calculated by integrating the product of the measured drain-source voltage ($v_{ds}$) and drain current ($i_d$) waveforms during turn-on ($t_{on}$) and turn-off ($t_{off}$ ) times whereas the total switching energy loss ($E_{total}$) is the sum of the turn-on ($E_{on}$) and turn-off ($E_{off}$ ) energy losses.
The switching power loss ($P_{sw}$) is obtained by multiplying the total switching energy loss of each device by switching frequency, as described by

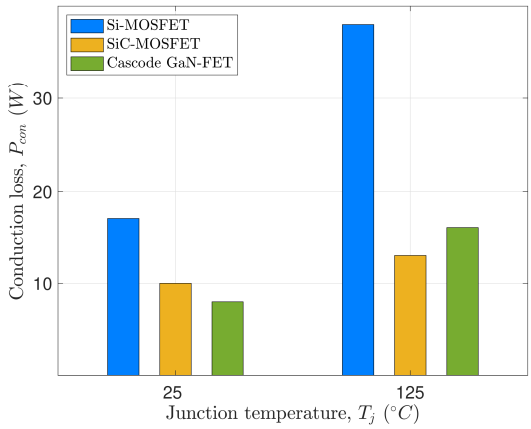


Fig. 9. Conduction loss of different devices at two junction temperatures.

$$E_{on} = \int_{ton} v_{ds}(t) i_d(t)\, dt \tag{9}$$

$$E_{off} = \int_{toff} v_{ds}(t) i_d(t)\, dt \tag{10}$$

$$E_{total} = E_{on} + E_{off} \tag{11}$$

$$P_{sw} = E_{total} f_{sw} \tag{12}$$

TABLE V
SWITCHING LOSS OF VARIOUS SEMICONDUCTOR DEVICES.

| Junction temperature | Switching power loss (W) Si MOSFET | SiC MOSFET | Cascode GaN-FET |
|---|---|---|---|
| $T_j$ = 25℃ | 21.5 | 10.5 | 9.0 |
| $T_j$ = 125℃ | 42.3 | 15 | 17.4 |

In Table V, the switching power loss for Si-MOSFET, SiC-MOSFET, and cascode GaN-FET is calculated at different junction temperatures while the switch current is 12 A. Fig. 10 presents that the switching loss for these devices is evaluated at the junction temperature of 25℃ when the switching frequency is increased from 50 to 150 kHz. It is noticed that cascode GaN-FET along with SiC-MOSFET exhibit a significantly lower switching power loss compared to Si-MOSFET at a higher junction temperature and higher switching frequency. This major reduction in loss results from a small delay time and a low rate of the *dv/dt* and *di/dt* during turn-on and turn-off transitions. Table VI shows a comparative evaluation of conduction and switching power losses for all devices at two junction temperatures of 25 and 125℃ while the switch current is 12 A and the switching frequency is 50 kHz. Obviously, cascode GaN-FET and SiC-MOSFET provide higher operating capabilities with remarkably lower conduction and switching losses among other devices.

## V. HARD-SWITCHING CHARACTERIZATION OF POWER DEVICES

It is important to understand the device switching characteristic and performance in order to employ different semiconductor devices in power converters. So, this section assesses and compares the dynamic characteristics of Si-MOSFET, SiC-MOSFET, and cascode GaN-FET in terms

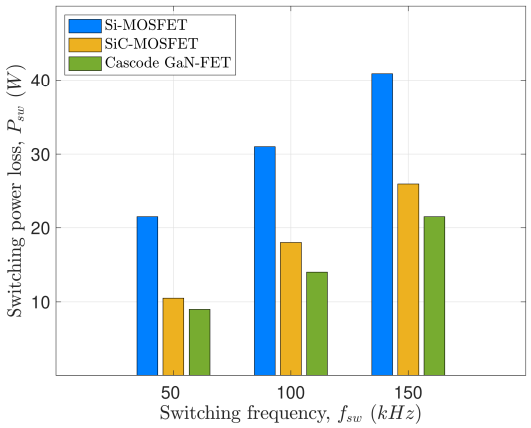


Fig. 10. Switching power loss for different power devices as the switching frequency is increased from 50 to 150 kHz and the switch current is 12 A.

TABLE VI
CONDUCTION AND SWITCHING POWER LOSSES FOR DIFFERENT POWER DEVICES.

| Semiconductor device | Loss | $T_j$ = 25℃ | $T_j$ = 125℃ |
|---|---|---|---|
| Si-MOSFET | $P_{con}$ | 17.3 W | 38.9 W |
| | $P_{sw}$ | 21.5 W | 42.3 W |
| SiC-MOSFET | $P_{con}$ | 9.4 W | 12.9 W |
| | $P_{sw}$ | 10.5 W | 15.0 W |
| Cascode GaN-FET | $P_{con}$ | 7.2 W | 15.2 W |
| | $P_{sw}$ | 9.0 W | 17.4 W |

of switching performance and energy loss. The impacts of operating conditions such as a gate resistance, switch current, and junction temperature, and DC-bus voltage on the switching device behavior are evaluated in terms of energy losses. The experimental results are analyzed and compared between the three different devices.

The switching performance of these devices are investigated and characterized under the hard-switching condition through the standard inductive-clamped load test circuit, which is known as DPT. The selected power devices have identical package structure to ensure that they have the exact parasitic inductance and capacitance effects. The gate-source voltage and gate resistance of the devices provided in the manufacturer's datasheet are taken into consideration for the evaluation. Due to the nearly zero reverse-recovery effects, the SiC-Schottky diode is employed in the DPT circuit to obtain a freewheeling path for the inductor current as well as to improve the switching behavior of the two power devices during the turn-on and turn-off transitions [55], [56].

### *A. Si-MOSFET Switching Waveforms*

The drain-source voltage ($V_{ds}$) and drain current ($I_d$) of the Si-MOSFET is studied to evaluate its switching behavior during the turn-on and turn-off transitions at the input voltage of 360 V, switch current of 12 A, and operating temperature of 25℃. The 650 V, 40 A Si-MOSFET device is tested with a gate-source ($V_{gs}$) voltage of –5 to +15 V for the turn-on and turn-off transitions while the turn-on ($R_{g(on)}$) and turn-off ($R_{g(off)}$) gate resistance values are 15 and 5 Ω to obtain an optimal low switching energy loss along with a small overshoot. This device features fast switching speeds with relatively low on-state resistance.

Figs. 11 and 12 show the drain-source voltage, drain current, gate-source voltage, and energy loss waveforms of the Si-MOSFET during the turn-on and turn-off events. The drain current waveform exhibits a high overshoot of 11 A along with a clear ringing in current and voltage waveforms during the turn-on transition due to the capacitance of the diode. In this event, the time-on is 80 ns while the *dv/dt* and *di/dt* are 6.9 kV/µs and 0.9 kA/µs, respectively. During the turn-off transition, there is a considerable overshoot of 132 V along with a large ringing in both the drain-source voltage and drain current waveforms due to the stray inductance, which can be minimized by controlling the current commutation loop. In this event, the time-off is 92.8 ns while the *dv/dt* and *di/dt* are 48 kV/µs and 1.5 kA/µs, respectively. The measured turn-on and turn-off energy losses are 94 and 30 µJ, respectively.

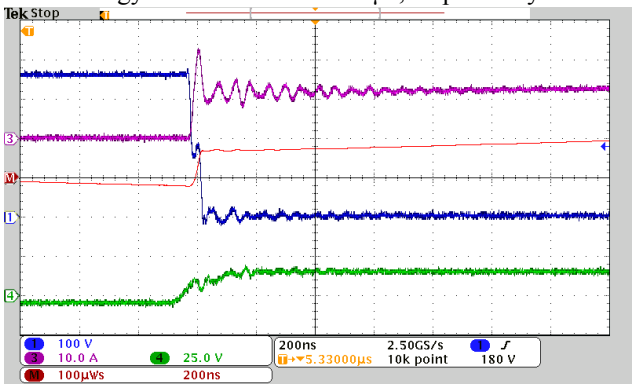


Fig. 11. Turn-on waveforms of Si-MOSFET with $V_{gs}$ = –5/+15 V, $R_{g(on)}$ = 15 Ω, and $R_{g(off)}$ = 5 Ω when $V_{ds}$ = 360 V and Id = 12 A.

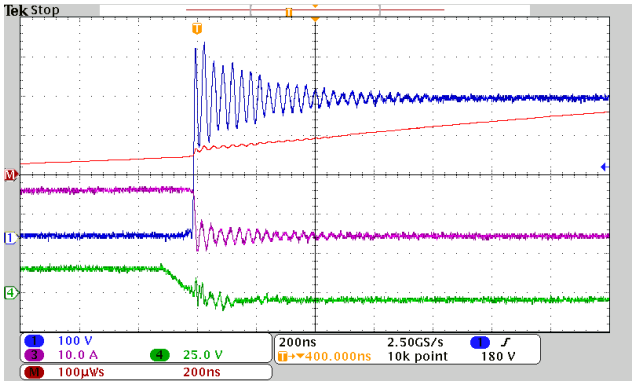


Fig. 12. Turn-off waveforms of Si-MOSFET with $V_{gs}$ = –5/+15 V, $R_{g(on)}$ = 15 Ω, and $R_{g(off)}$ = 5 Ω when $V_{ds}$ = 360 V and $I_d$ = 12 A.

### *B. SiC-MOSFET Switching Waveforms*

The drain-source voltage and the drain current of the SiC-MOSFET is tested to evaluate its switching behavior during the turn-on and turn-off transitions at the input voltage of 360 V, switch current of 12 A, and operating temperature of 25℃. The 650 V, 39 A SiC-MOSFET device operates at a gate-source voltage of –5 to +15 V for the turn-on and turn-off transitions when the turn-on and turn-off gate resistance values are set at 15 and 5 Ω to reduce switching energy loss and improve switching behavior. The prime advantages of this device are a low on-state resistance, small gate charge, and high switching frequency with fast reverse recovery.

Figs. 13 and 14 depict the drain-source voltage, drain current, gate-source voltage, and energy loss waveforms of the SiC-MOSFET during the turn-on and turn-off events. The drain current waveform shows a small overshoot of 6 A along with a very slightly ringing in current waveform during the turn-on transition due to the reverse recovery charge of the body diode. In this event, the time-on is 82 ns when the *dv/dt* and *di/dt* are 3.5 kV/µs and 0.4 kA/µs, respectively. During the turn-off transition, there is a large overshoot of 112 V along with a considerable ringing in both the drain-source voltage and drain current waveforms due to the parasitic effects. In this event, the time-off is 54 ns when the *dv/dt* and *di/dt* are 11.1 kV/µs and 0.3 kA/µs, respectively. The measured turn-on and turn-off energy losses are 96 and 52 µJ, respectively.

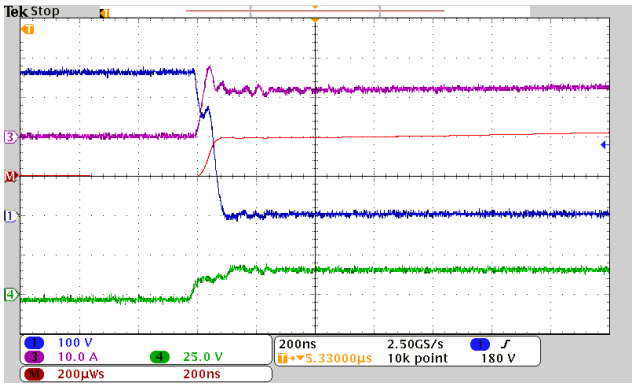


Fig. 13. Turn-on waveforms of SiC-MOSFET with $V_{gs}$ = –5/+15 V, $R_{g(on)}$= 15Ω, and $R_{g(off)}$ = 5Ω when $V_{ds}$ = 360 V and $I_d$ = 12 A.

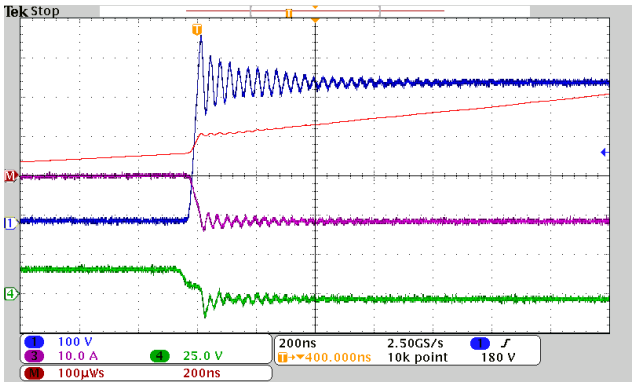


Fig. 14. Turn-off waveforms of SiC-MOSFET with $V_{gs}$ = –5/+15 V, $R_{g(on)}$= 15Ω, and $R_{g(off)}$ = 5 Ω when $V_{ds}$ = 360 V and $I_d$ = 12 A.

### C. Cascode GaN-FET Switching Waveforms

The drain-source voltage and the drain current of the cascode GaN-FET is examined to assess its switching behavior during the turn-on and turn-off transitions at the input voltage of 360 V, switch current of 12 A, and operating temperature of 25℃. The 650 V, 46.5 A cascode GaN-FET device operates at a gate-source voltage of –5 to +15 V for the turn-on and turn-off events while the turn-on and turn-off gate resistance values are 15 and 5 Ω to reduce switching energy loss and enhance switching behavior. The main advantages of this device are low on-state resistance, high-switching speed, and small-intrinsic capacitance with ultra-low reverse recovery charge.

Figs. 15 and 16 depict the drain-source voltage, drain current, gate-source voltage, and energy loss waveforms of the cascode GaN-FET during the turn-on and turn-off events. Noteworthy, the drain current waveform shows a large overshoot of 15 A along with a major ringing in current and voltage waveforms during the turn-on transition due to the reverse recovery charge of the body diode in the low voltage MOSFET that is embedded inside the cascode GaN device as well as the high Miller effects. In this event, the time-on is 50 ns while the *dv/dt* and *di/dt* are 48 kV/µs and 1.3 kA/µs, respectively. In the turn-off transition, there is a small overshoot of 36 V along with a very small ringing in both the drain-source voltage and drain current waveforms due to the cascode configuration and capacitance charge. In this event, the time-off is 60 ns while the *dv/dt* and *di/dt* are 23.2 kV/µs and 0.7 kA/µs, respectively. The measured turn-on and turn-off energy losses are 29 and 22 µJ, respectively.

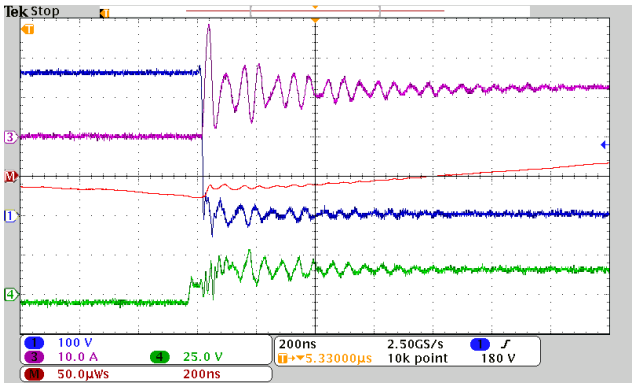


Fig. 15. Turn-on waveforms of cascode GaN-FET with $V_{gs}$ = –5/+15 V, $R_{g(on)}$ = 15Ω, and $R_{g(off)}$ = 5Ω when $V_{ds}$ = 360 V and $I_d$ = 12 A.

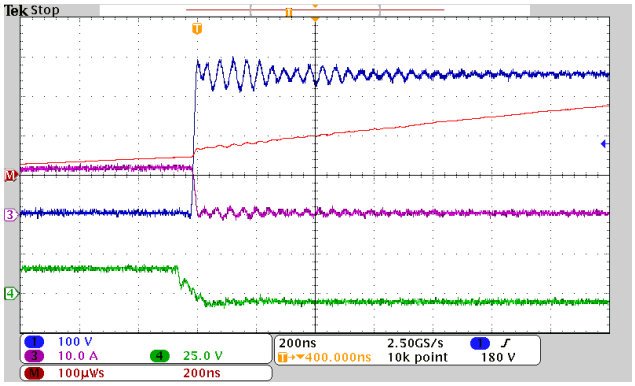


Fig. 16. Turn-off waveforms of cascode GaN-FET with $V_{gs}$ = –5/+15 V, $R_{g(on)}$ = 15Ω, and $R_{g(off)}$ = 5Ω when $V_{ds}$ = 360 V and $I_d$ = 12 A.

### D. Switching Behavior Comparison

Based on the experimental results, the cascode GaN-FET exhibits considerably reduced switching energy loss compared to Si-MOSFET and SiC-MOSFET because the switching time during the turn-on and turn-off transitions is much shorter than Si and SiC devices. Though the overshoot and ringing effects in the cascode GaN-FET are notable due to high *dv/dt* and *di/dt* across the parasitic elements during the turn-on event, the Si-MOSFET and SiC-MOSFET shows a very large overshoot and ringing phenomenon in both the drain-source voltage and drain current waveforms during the turn-off event. The d*v/dt* and *di/dt* of Si and SiC devices are larger than those in the cascode GaN-FET device during the turn-off event.

## VI. Switching Energy Loss Assessment

The switching energy losses of Si-MOSFET, SiC-MOSFET, and cascode GaN-FET are assessed at various operating conditions of gate resistance values, switch currents, junction temperatures, and DC-bus voltages. These devices are examined at the same gate requirements to distinguish their switching performance. In the meantime, the gate-driver of Infineon (1EDI60I12AH) is used for driving each device as the gate-source voltage is –5/+15 V.

### *A. Switching Assessment at Different Gate Resistance Values*

Gate resistance has a significant impact on the switching performance of devices. The energy loss dramatically increases at higher gate resistance so lowering gate resistance reduces the transient time of the switching device. This process can help to minimize the energy loss; nevertheless, a smaller gate resistance can increase the overshoot and ringing of device voltage and current during turn-on and turn-off transitions. The choice of gate resistance is a critical factor for the proper switching operation of power devices. Therefore, Si-MOSFET, SiC-MOSFET and cascode GaN-FET are examined at different gate resistance values and each device is operated at 360 V and 12 A.

The turn-off gate resistance is elevated from 5 to 25 Ω while the turn-on gate resistance stays at a fixed value of 5 Ω. The top Fig. 17 illustrates that the turn-off energy losses for power devices are almost constant as increasing the turn-off gate resistance value. At the turn-off gate resistance of 25 Ω, turn-off losses of Si-MOSFET, SiC-MOSFET and cascode GaN-FET are 34, 30, and 22 µJ, respectively. The bottom Fig. 17 shows a major increase in turn-on losses for each device as the turn-on gate resistance is increased from 5 to 25 Ω while the turn-off gate resistance remains fixed at 5 Ω. However, the turn-on loss of the cascode GaN-FET increases slightly with increasing the turn-on gate resistance. At the turn-on gate resistance of 25 Ω, turn-on losses of Si-MOSFET, SiC-MOSFET and cascode GaN-FET are 220.2, 160.5, and 110.1 µJ, respectively. Thus, the cascode GaN-FET remarkably reduces the switching energy loss by 31.4% compared to SiC-MOSFET and by 50% compared to Si-MOSFET at a higher turn-on gate resistance during the turn-on transition. This means that the changing gate resistance value has a major impact only on the turn-on energy losses for both devices.

Table VII shows the total energy loss comparison for all devices at various gate resistances. The effect of changing gate resistances on each switching device is evaluated through the DPT circuit during turn-off and turn-on transitions. Different gate resistances have a notable influence on both switching performance and energy loss of power devices during the two switching transitions. Reducing the turn-off and turn-on gate resistances can decrease the switching time and loss, causing high the *dv/dt* and *di/dt* rates with large oscillation and overshoot in the device voltage and current waveforms.

Figs. 18 and 19 show *dv/dt* and *di/dt* rates of each device at various gate resistances during the turn-off and turn-on transitions. The d*v*/d*t* and *di/dt* rates for Si-MOSFET, SiC-MOSFET, and cascode GaN-FET are reduced by increasing gate resistance values. Among these devices, the

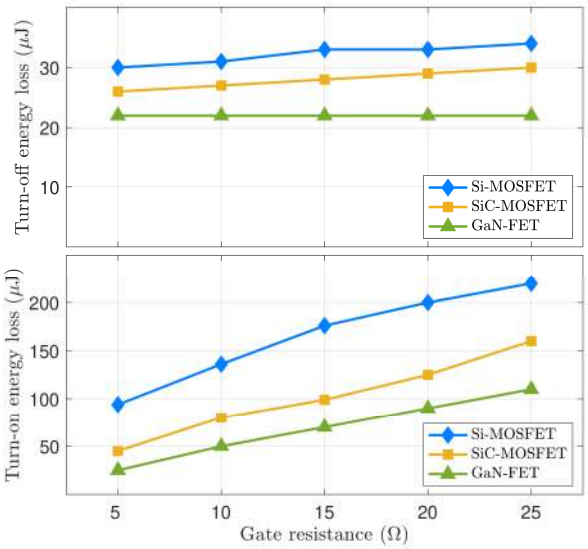


Fig. 17. Turn-off and turn-on energy losses of Si-MOSFET, SiC-MOSFET, and cascode GaN-FET as the gate resistance is increased from 5 to 25 Ω.

TABLE VII
TOTAL ENERGY LOSS OF TESTED POWER DEVICES AT DIFFERENT GATE RESISTANCE VALUES.

| | Total energy loss (µJ) | | |
|---|---|---|---|
| Gate resistance (Ω) | Si MOSFET | SiC MOSFET | Cascode GaN-FET |
| 5.0 | 124.7 | 71.2 | 47.4 |
| 10 | 167.0 | 110.6 | 75.3 |
| 15 | 209.4 | 124.9 | 89.5 |
| 20 | 233.6 | 154.2 | 112.0 |
| 25 | 254.2 | 190.5 | 132.1 |

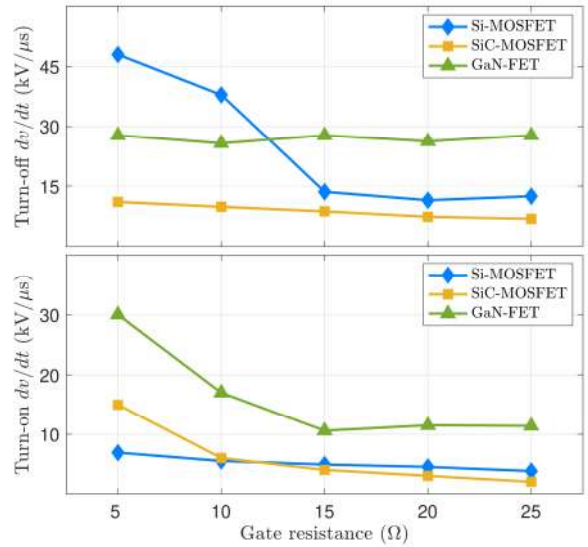


Fig. 18. Turn-off and turn-on *dv/dt* of Si-MOSFET, SiC-MOSFET, and cascode GaN-FET as the gate resistance is increased from 5 to 25 Ω.

cascode GaN-FET exhibits higher rates because of cascode structure of GaN device as well as high stray parasitic elements and faster switching frequency. To mitigate the high d*v*/d*t* and d*i*/d*t* rates in the switching performance of the cascode GaN-FET, the gate resistance during the turn-off and turn-on transitions should be increased. Thus, it is crucially important to obtain the optimal gate resistance value for each semiconductor device employed in the power converter design.

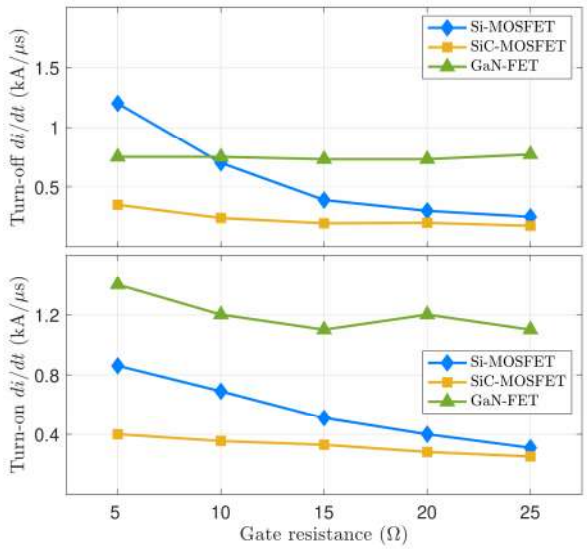


Fig. 19. Turn-off and turn-on *di/dt* of Si-MOSFET, SiC-MOSFET, and cascode GaN-FET as the gate resistance is increased from 5 to 25 Ω.

### B. *Switching Assessment at Different Switch Currents*

Si-MOSFET, SiC-MOSFET and cascode GaN-FET are performed under the input voltage of 360 V and junction temperature of 25℃ as the switch current is increased from 4 to 12 A. Based on the experimental measurement, the switching energy losses of the Si-MOSFET and SiC-MOSFET, especially in turn-on loss, are drastically high due to Miller current effect. Fig. 20 illustrates the total switching energy loss for Si-MOSFET, SiC-MOSFET, and cascode GaN-FET at different switch currents, showing their effects on the total energy loss. As the switch current increases, the total energy loss of the two devices increases linearly. Although the energy loss of each device is increased, the total energy loss for the Si-MOSFET and SiC-MOSFET is clearly two times more than the total energy loss for the GaN-FET, particularly after the switch current is exceed 8 A. At the switch current of 12 A, the cascode GaN-FET outstandingly decreases total energy loss by 63.1.8% compared to the Si-MOSFET and by 57.8% compared to the SiC-MOSFET. As a result, GaN device is capable of operating at a higher current with much lower energy loss.

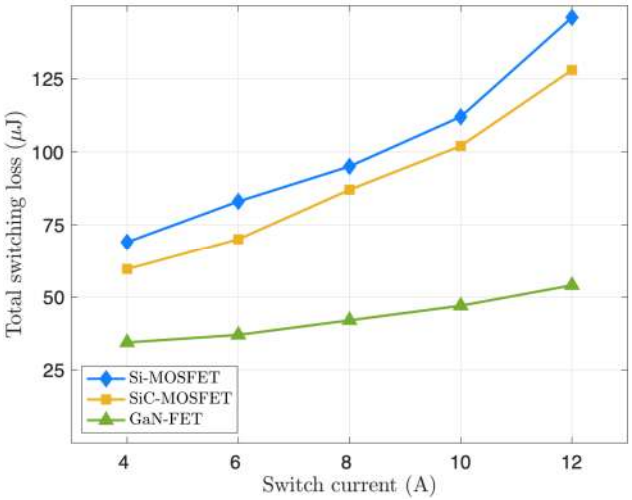


Fig. 20. Total switching energy loss of Si-MOSFET, SiC-MOSFET, and cascode GaN-FET as the switch current is increased from 4 to 12 A.

### C. *Switching Assessment at Different Junction Temperatures*

To investigate the effect of high operating temperatures, the hotplate is used to heat only the device under test while the entire DPT circuit is placed in the room temperatures. For the safe operation, the heat sink of the tested device is connected to the hot plate by an external heat sink in order to increase the operation temperature. Table VIII shows that total energy loss of each device increases as the junction temperature is increased from 25 to 125℃. It is clear that the total energy loss of all power devices increases significantly with increasing junction temperature. However, the cascode GaN-FET and SiC-MOSFET achieve remarkably lower total energy loss compared to the Si-MOSFET throughout different junction temperatures. At the temperature of 125℃, Fig. 21 shows that the total energy loss of the SiC-MOSFET has the lowest total energy loss because of its better thermal conductively and melting points compared to other semiconductor materials. Obviously, that WBG devices exhibit excellent switching performance with lower energy losses at higher operating temperatures.

TABLE VIII
TOTAL ENERGY LOSS OF TWO TESTED DEVICES AT DIFFERENT JUNCTION TEMPERATURES.

| | Total energy loss (μJ) at | | |
|---|---|---|---|
| Device | $T_j$ = 25℃ | $T_j$ = 75℃ | $T_j$ = 125℃ |
| Si-MOSFET | 11.6 | 190.3 | 242.5 |
| SiC-MOSFET | 74.3 | 129.7 | 192.4 |
| GaN-FET | 60.4 | 130 | 208.7 |

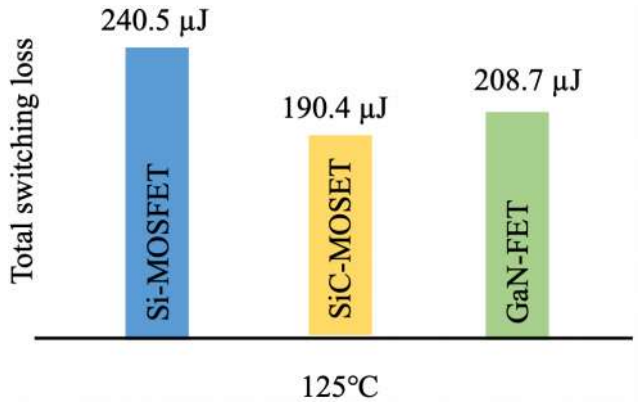


Fig. 21. Total switching energy loss of Si-MOSFET, SiC-MOSFET, and cascode GaN-FET at the junction temperature of 125℃.

### D. *Switching Assessment at Different DC-bus Voltages*

The switching energy losses of Si-MOSFET, SiC-MOSFET, and cascode GaN-FET are assessed at the switch current of 10 A and junction temperature of 25℃ as a function of increasing DC-bus voltage. Fig. 22. shows a comparison of the turn-on, turn-off, and total energy losses as the DC-bus voltage is increased from 200 to 360 V. The switching energy losses are measured by integrating the instantaneous power during a commuted interval. The energy losses for Si-MOSFET, SiC-MOSFET, and cascode GaN-FET increase in conjunction with increasing the DC-bus voltage. However, the cascode GaN-FET exhibits a lower total energy loss as the DC-bus voltage increases. At the DC-bus voltage of 360 V and switch current of 10 A, the cascode GaN-FET reduces the total energy

loss by nearly 65% compared to the Si-MOSFET and by almost 60% compared to the SiC-MOSFET. Therefore, GaN device provides improved switching performance along with considerably reduced energy losses at a higher voltage.

## VII. BIDIRECTIONAL CONVERTER EVALUATION

The objective of this section is to demonstrate the effects of merging various new semiconductor devices into power converters. The switching performance of cascode GaN-FETs, SiC-MOSFETs, and Si-MOSFETs employed in the bidirectional converter is examined with the same power converter layout. The semiconductor losses, including conduction and switching losses, occurred in power devices are analyzed and compared at various operating temperatures and switching frequencies. The overall performance of the GaN based converter is experimentally evaluated at harsh operating conditions and compared it to Si-based and SiC-based converters in terms of total power loss, energy efficiency, and cost in order to realize the benefits of using GaN technology.

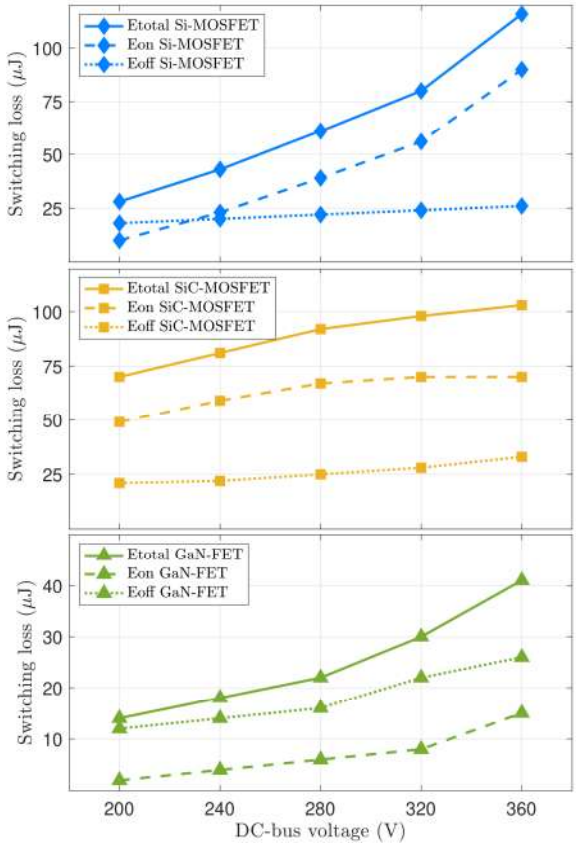


Fig. 22. Switching energy loss of Si-MOSFET, SiC-MOSFET, and cascode GaN-FET as the DC-bus voltage is increased from 200 to 360 V.

### A. Converter Performance Evaluation

To evaluate the impacts of using different semiconductor device technologies on power converters in terms of switching performance, total power loss, and energy efficiency, three bidirectional dc–dc buck-boost converters are built and examined: the first one is constructed with traditional Si-MOSFETs and Si-diodes, the second one is constructed with common SiC-MOSFETs and SiC-Schottky diodes, and the third one is constructed with new cascode GaN-FETs and SiC-Schottky diodes. These converters are assessed at various switching frequencies, input voltages, load currents, and output power levels, which are the most crucial operating parameters in power conversion applications. SiC-Schottky diodes (C3D16065D1) are incorporated in used in WBG based converters because these diodes have the remarkable advantages of a higher blocking voltage, ultra-faster switching speed, and virtually zero reverse-recovery loss compared to Si-diodes (IDW30C65D1).

### B. Converter Switching Evaluation

Further detailed investigation and analysis are necessitated for medium-voltage power converter applications in order to demonstrate tradeoffs in switching performance and converter efficiency when substituting GaN devices for Si and SiC counterparts, especially in a cascode configuration. Therefore, A prototype of 500 W bidirectional converter is implemented to validate the impacts of emerging medium-voltage cascode GaN devices on the converter performance and efficiency. Under identical operating conditions, the three bidirectional converters with different semiconductor devices are experimentally evaluated in terms of current and voltage overshoots, switching times, and switching energy losses, especially during the turn-on transition. The switching performance of each converter highly depends on the gate requirements of power devices; therefore, the gate-source voltage and gate resistance of each device integrated into the bidirectional converter are listed in Table IX, taking the manufacture's datasheet into considerations.

TABLE IX
GATE REQUIREMENTS FOR IMPLEMENTED POWER DEVICES.

| Parameters | Gate requirements for | | |
|---|---|---|---|
| | Si-MOSFET | SiC-MOSFET | Cascode GaN-FET |
| $V_{gs}$ | –4/+14 V | –5/+18 V | -5/+15 V |
| $R_{off}$ | 5 Ω | 5 Ω | 5 Ω |
| $R_{on}$ | 20 Ω | 20 Ω | 15 Ω |

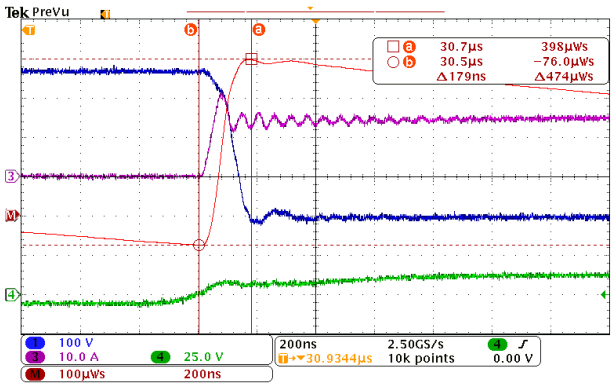


Fig. 23. Turn-on waveforms of Si-based converter at $V_{gs}$ = –4/+14 V, $R_{g(on)}$= 20 Ω, and $R_{g(off)}$ = 5 Ωwhen $V_{in}$ = 360 V and $I_{load}$ = 12 A.

The turn-on switching waveforms of Si-MOSFET, SiC-MOSFET and cascode GaN-FET devices integrated into the bidirectional converter are evaluated and compared at the switching frequency ($f_{sw}$) is 40 kHz. Figs. 23, 24, and 25 illustrate the switching performance of three bidirectional

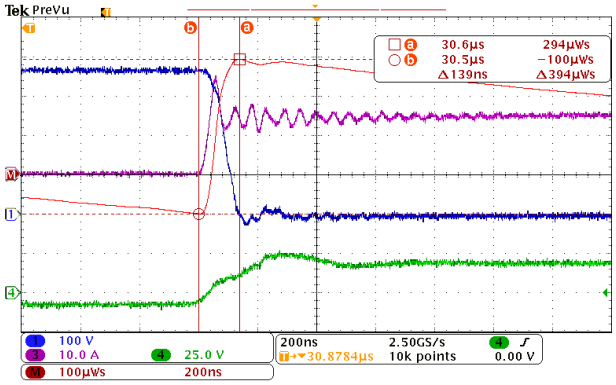


Fig. 24. Turn-on waveforms of SiC-based converter at $V_{gs}$ = –5/+18 V, $R_{g(on)}$= 20 Ω, and $R_{g(off)}$ = 5 Ω when $V_{in}$ = 360 V and $I_{load}$ = 12 A.

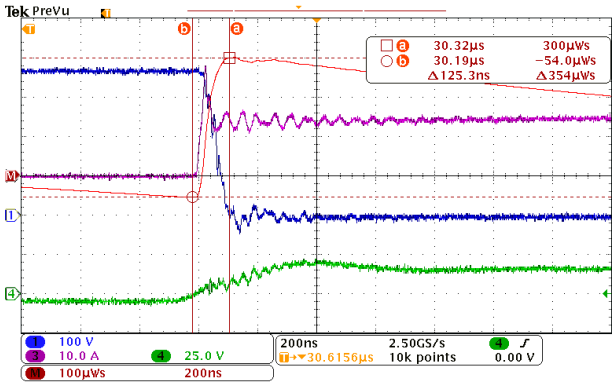


Fig. 25. Turn-on waveforms of GaN-based converter at $V_{gs}$ = –5/+15 V, $R_{g(on)}$ = 20 Ω, and $R_{g(off)}$ = 5 Ω when $V_{in}$ = 360 V and $I_{load}$ = 12 A.

converters during the turn-on transition. It is noticed that the current waveform for Si-based, SiC-based, and GaN-based converters exhibits a large overshoot and high oscillation due to the high rate of $di/dt$ in the turn-on event. Because of the faster switching speed and shorter switching time for cascode GaN-FET device, the GaN-based converter reveals a considerably lower turn-on energy loss, which is 354 µJ, while the turn-on energy losses for Si-based and SiC-based converters are 474 and 394 µJ, respectively.

### C. Converter Power Loss Evaluation

Power loss analysis is one of the important steps to evaluate various semiconductor devices implemented in the bidirectional converter. To determine conduction and switching losses of each device, the on-state resistance is obtained from the device's datasheet while the energy loss is measured through the DPT during the turn-on and turn-off transitions. Total power loss is calculated by the sum of the switching power and conduction losses of the switch and conduction loss of the diode along with other loss such as passive and gate-driver losses. It is noteworthy that the duty cycle is considered in the power loss evaluation. Total power loss is represented as:

$$P_{total} = P_{S,sw} + P_{S,con} + P_{D,con} + P_{passive} + P_{gate} \quad (13)$$

where $P_{S,sw}$ is the switching power losses during turn-on and turn-off events of each switch while $P_{S,con}$ and $P_{D,con}$ are the conduction loss for the switch and diode. $P_{passive}$ and $P_{gate}$ are the passive element loss and gate-driver losses, respectively.

Total loss of Si-MOSFETs/Si-diodes, SiC MOSFETs/SiC-Schottky diodes, and cascode GaN-FETs/SiC-Schottky diodes incorporated into the bidirectional converter is determined when the converter system is performed at an output power of 500 W, a switching frequency of 100 kHz, and an operating temperature of 25℃ Fig. 26 depicts a comparison of total power loss between Si-based, SiC-based, GaN-based bidirectional converters. Compared to Si-based and SiC-based converters, the GaN-based converter has a substantially lower total power loss due to smaller on-state resistance and shorter switching times.

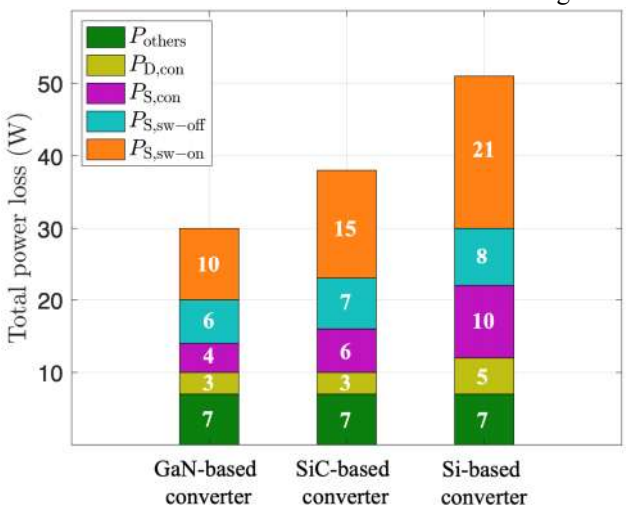


Fig. 26. Total power loss of each bidirectional converter.

### D. Converter Efficiency Evaluation

This section is presented the efficiency measurement approach along with the converter efficiency evaluation at differ-ent operating conditions. The method of measuring converter efficiency plays key role in evaluating the converter performance using various semiconductor devices. To obtain accu-rate results, the voltage and current should be simultaneously measured at the input-side and output-side of the converter. Among diverse efficiency measurement processes, the power analyzer (P2022A), made by Keysight, significantly provides higher measurement accuracy and flexibility in the converter connection. This power analyzer with precision internal shunt current and high differential voltage probes is used to achieve an accurate measurement efficiency for bidirectional dc–dc converters.

The power analyzer is remarkably operated as an oscilloscope in order to visualize current and voltage along with power waveforms in the real-time event, reducing a separated oscilloscope in the measurement arrangement. At the steady-state period, the current and voltage at both input-side and output-side of converter system are measured at the same time to gain the instantaneous power and overall converter efficiency. Fig. 27 shows a prototype of the 500 W bidirectional dc–dc buck-boost converter. Overall converter efficiency ($\eta$) is computed by dividing the output power ($P_{out}$) by the input power ($P_{in}$), as follows

$$\eta = \frac{P_{out}}{p_{in}} \cdot 100\% \quad (14)$$

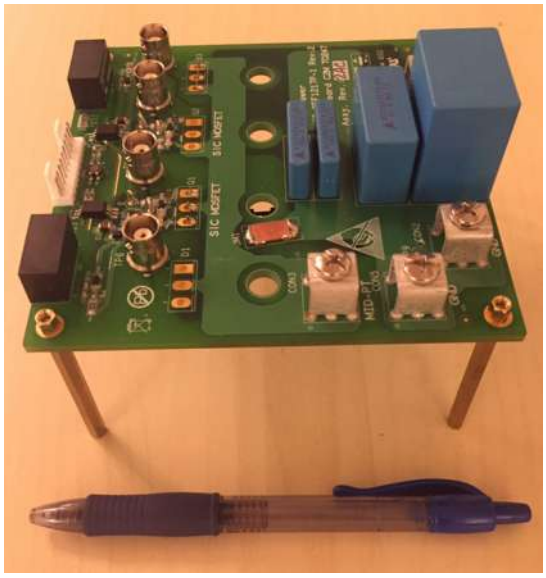

Fig. 27. Hardware prototype of the bidirectional dc–dc buck-boost converter.

In this section, the investigation on effects of integrating different semiconductor device technologies into power converters in energy efficiency is performed at harsh operating conditions. The efficiency of Si-based, SiC-based, and GaN-based converters is compared and evaluated as increasing of switching frequency, input voltage, and output power level are increased.

In diverse applications, there is an acute need for power electronics working at high switching frequencies, which considerably minimize the size of passive elements and reduce the volume of cooling systems. Therefore, the Si-based, SiC-based, and GaN-based converters are examined at fast switching speeds. In the examination, the passive components, capacitors and inductors, are optimized to handle the increase of a high switching frequency. Fig. 28 shows the efficiency of the three tested converters as the switching frequency increases gradually from 40 to 200 kHz at an input voltage of 96 V and a junction temperature of 25℃. As the switching speed increases, the efficiency of the Si-based converter decreases dramatically due to higher conduction and switching losses while SiC-based and GaN-based converters offer better efficiency level.

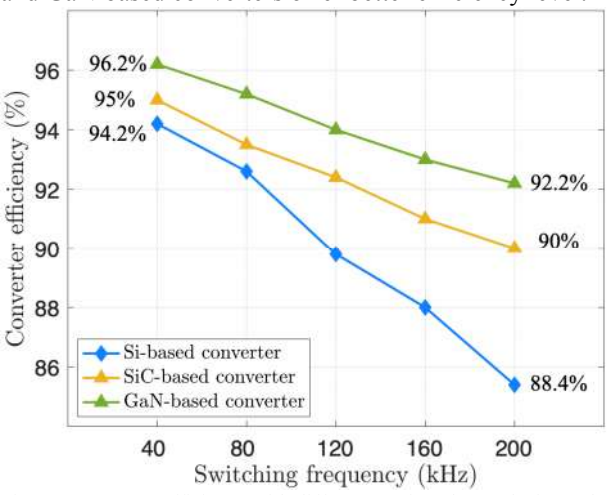


Fig. 28. Converter efficiency with different semiconductor device technologies as a function of increasing switching frequency from 40 to 200 kHz at an input voltage of 96 V.

It is observed the GaN-based converter achieves 92.2% efficiency while the SiC-based converter reaches only 90% efficiency and the Si-based converter can barely have 88.4% at a switching frequency of 200 kHz. The results show that cascode GaN-FETs along with SiC-Schottky diodes substantially improves the overall converter efficiency by 2.44% compared to the SiC-based converter and by nearly 8% compared to the Si-based converter. Thus, integrating GaN power devices into the bidirectional dc–dc converter provides beneficial effects in terms of loss reduction and efficiency improvement.

The input voltage of the bidirectional converter is a pivotal factor in energy storage and renewable energy applications because the voltage can be changeable based on operating condition of power operation systems for supplying or storing electric energy. Therefore, the performance of each converter is assessed to measure the energy efficiency over a wide range of input voltages.

It is noteworthy that the bidirectional converter is constructed to operate effectively around the designed input voltage. This means that the converter performance obtains peak efficiency at the input voltage of 96 V. As the input voltage is increased from 48 to 96 V, the efficiency of three converters is compared at a switching frequency of 40 kHz, as shown in Fig. 29. SiC-based and GaN-based converters provide a higher efficiency level while the Si-based is struggling to reach better efficiency because of its larger conduction and switching losses, especially at higher input voltages. Among three bidirectional converters, the converter using GaN-FETs and SiC-Schottky diodes achieves 96.2% efficiency, which is considerably higher than efficiency of both Si-based and SiC-based converters. At the input voltage of 96 V, GaN power device technology remarkably enhances converter efficiency by 1.3% compared to the SiC-based converter and by 2.2% compared to the Si-based converter. As a result, the combination of cascode GaN-FETs and SiC-Schottky diodes is enabling power converter to perform efficiently even at higher input voltages.

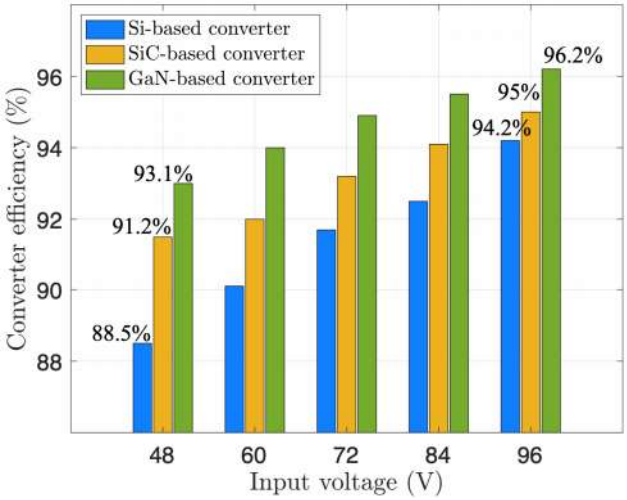


Fig. 29. Converter efficiency with different power devices as increasing input voltage from 48 to 96 V at a switching frequency of 40 kHz.

The performance of the Si-based, SiC-based, and GaN-based

converters is evaluated at a wide range of output power levels, which can play an important role in power conversion systems. The input and output powers of each converter are measured through current and voltage probes to determine their efficiency level, which is computed by the power analyzer at two switching frequencies of 100 and 200 kHz. Each bidirectional converter works efficiently around 300 and 400 W, as the designed power rating. Thus, the converter reaches peak efficiency at output power levels of 300 and 400 W. Fig. 30 shows the efficiency comparison of Si-based, SiC-based, and GaN-based converters when the output power level is increased from 100 to 500 W at two different switching speeds. SiC-based and GaN-based converters offer better efficiency level throughout different output powers compared to the Si-based converter. After 400 W, the converter efficiency with Si devices drops drastically while the GaN-based converter 94% efficiency, which is higher than the other two converters. Even though the converter works at higher output power levels, the combination of cascode GaN-FETs and SiC-Schottky diodes can still preserve the converter at higher efficiency level. At 200 kHz, it is noticed that efficiency of the GaN-based converter only reduced by 1.1% while efficiency of Si-based and SiC-based converters decreased dramatically by 2.4% and 4.6%, respectively. Thus, integrating GaN-FETs into the converter can noticeably increase the efficiency due to the superior material properties and high operating capabilities of GaN technology.

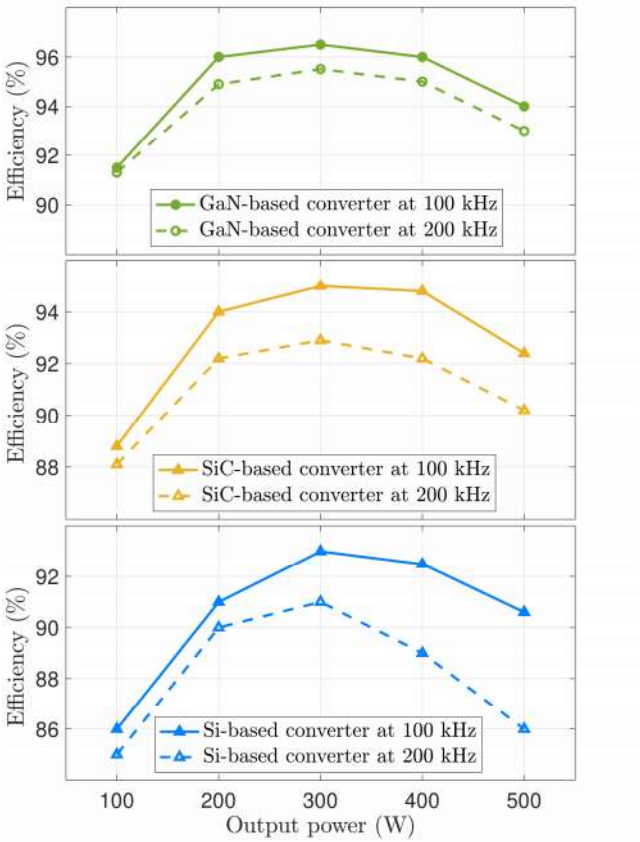


Fig. 30. Converter efficiency using different semiconductor devices with increasing output power level from 100 to 500 W at two switching frequencies of 100 and 200 kHz.

## VIII. MARKET PRICE COMPARISON FOR POWER DEVICES

The cost of power devices is an important factor in power converter applications; therefore, this section investigates the market price between different semiconductor devices incorporated into the bidirectional dc–dc converters. Si-MOSFETs, SiC-MOSFETs, and cascode GaN-FETs from various semi-conductor manufacturers are compared in terms of their price and availability in the market. The price comparison for these implemented devices was performed at a certain time period, which was in the first quarter of 2020 (January 1 – March 31) because the price of semiconductor devices is varied due to the time period and other market factors. In this comparison, the current rate, device package, and voltage level are taken into the consideration. Fig. 31 shows the average cost for three different device topologies as a function of increasing rating current and the price is collected from different semiconductor distributors. It is realized that the price of GaN semiconductors is the most expensive devices among device technologies since GaN power devices are relatively new candidates in the market. Based on the main suppliers, such as Digi-key and Mouser, the actual price for power devices implemented in the three bidirectional converters is listed in Table X. It is noticed that the price for the first combination of Si-MOSFETs and Si-diodes is $24.98 while the price in the second combination of SiC-MOSFETs and SiC-Schottky diodes is $34 and the price for the third combination of cascode GaN-FETs and SiC-Schottky diodes is $50.46. It shows that the GaN-based converter is costly, which is two times higher than the Si-based converter while the SiC-based converter is relatively expensive. However, several recent published studies, such as [57] and [58], illustrate the market and trend of price for GaN devices. These studies show that GaN power devices have been gradually decreased due to a rapidly developing GaN technology and increasing number of GaN semiconductor manufacturers.

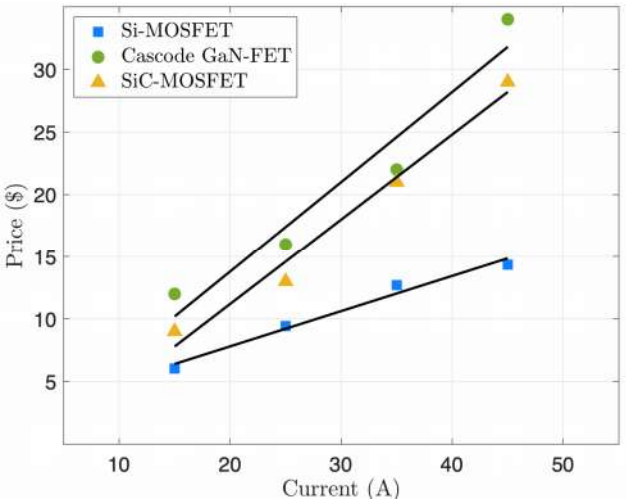


Fig. 31. Price comparison between Si-MOSFET, SiC-MOSFET, and cascode GaN-FET devices at various rating currents in the first quarter of 2020.

In spite of the fact that the price of GaN power devices is more expensive compared to the Si and SiC counterparts, GaN device technology offers remarkably more than 45% reduction

in switching energy losses, leading to enhance the switching performance of the converter. Cascode GaN-FET devices feature high operating capabilities, which are enabling power converters to work effectively at harsh operating conditions of switching frequency, junction temperature, and output power level. Since GaN devices are able to operate at higher switching speeds compared to other device technologies, the size of passive elements as well as volume of cooling systems used in power converters can be greatly minimized, resulting a significant reduction in total power loss and weight of the bidirectional converter. The converter using cascode GaN-FET devices is more robust and efficient than other converters. It also exhibits a significantly higher efficiency level with lower the converter size even at cruel operating conditions. As a result, the high price of GaN devices can be reasonably compensated by implementing smaller passive components, such as capacitors and inductors, and lower cooling systems in power converters, which can majorly improve the converter performance as well as increase the energy efficiency.

TABLE X
PRICE COMPARISON FOR VARIOUS POWER DEVICE TECHNOLOGIES USED IN THE BIDIRECTIONAL DC–DC CONVERTER.

| | Combination (1) (Si-MOSFET/ Si-diode) IPW90R120C3/ IDW30C65D1 | Combination (2) (SiC-MOSFET/ SiC-diode) (C3M0065090D/ C3D16065D1) | Combination (3) GaN-FET/ SiC-diode) (TP90H050WS/ C3D16065D1) |
|---|---|---|---|
| Switches ($S_1$,$S_2$) | 2 × $9.68 | 2 × $9.98 | 2 × $18.21 |
| Diodes ($D_1$, $D_2$) | 2× $2.81 | 2 × $7.02 | 2 × $7.02 |
| **Total cost** | **$24.98** | **$34** | **$50.46** |

## IX. CONCLUSION

This paper was experimentally evaluated the impact of integrating medium-voltage cascode GaN power devices into bidirectional dc–dc converters that are widely used in energy storage systems and renewable energy applications. The benefits of replacing Si and SiC devices with cascode GaN-FETs in power converter were demonstrated in terms of switching behavior, total power loss, energy efficiency, and cost. Si-based, SiC-based and GaN-based converters with the same design specifications were implemented to compare their performance under harsh operating conditions. The switching behavior as well as energy loss of Si-MOSFET, SiC-MOSFET and cascode GaN-FET power devices were examined through the DPT circuit as the gate resistance value, switch current, junction temperature, and DC-bus voltage increased. Compared to Si and SiC devices, the cascode GaN-FET exhibited outstanding switching characteristics with significantly lower energy losses, which greatly enhanced the switching performance of the converter. Furthermore, the total power loss for Si-based, SiC-based and GaN-based converters was analyzed to evaluate their efficiency over a wide range of switching speeds, input voltage, and output power levels. Because of smaller on-state resistance and shorter switching times of the cascode GaN-FETs besides GaN's superior material properties, the GaN-based converter exhibited a major reduction in power losses, leading to highly improve the energy efficiency even at cruel operating conditions. Although GaN devices are expensive, the high price of GaN devices can be reasonably compensated by using smaller passive components and cooling systems in power converters. The experimental results revealed considerable benefits to using cascode GaN-FET power devices in the bidirectional dc–dc converter at the medium-voltage level, which was improved substantially in terms of switching performance as well as converter efficiency

## REFERENCES


[1] H. Wu, K. Sun, L. Zhu, and Y. Xing, "An interleaved half-bridge three-port converter with enhanced power transfer cpability using three-leg rectifier for renewable energy applications," *IEEE J. of Emerging and Select. Topics in Power Electron*., vol. 4, no. 2, pp. 606–616, June 2016.

[2] M. Fan, K. Sun, D. Lane, W. Gu, Z. Li, and F. Zhang, "A novel generation rescheduling algorithm to improve power system reliability with high renewable energy penetration," *IEEE Trans. Power Syst*., vol. 33, no. 3, pp. 3349–3357, May 2018

[3] C. Ma, F. Gao, G. He, and G. Li, "A voltage detection method for the voltage ride-through operation of renewable energy generation systems under grid voltage distortion conditions," *IEEE Trans. Sustain. Energy*, vol. 6, no. 3, pp. 1131–1139, July 2015.

[4] A. Deihimi and M. E. S. Mahmoodieh, "Analysis and control of battery-integrated dc/dc converters for renewable energy applications," *IET Power Electron*., vol. 10, no. 14, pp. 1819–1831, 2017.

[5] T. Dragi˘cevi´c, X. Lu, J. C. Vasquez, and J. M. Guerrero, "DC microgrids–part I: A review of control strategies and stabilization techniques," *IEEE Trans. on Power Electron*., vol. 31, no. 7, pp. 4876–4891, 2016.

[6] T. Dragi˘cevi´c, X. Lu, J. C. Vasquez, and J. M. Guerrero, "DC microgrids–part II: a review of power architectures, applications, and standardization issues," *IEEE Trans. on Power Electron*., vol. 31, no. 5, pp. 3528–3549, May 2016.

[7] O. Cornea, G. Andreescu, N. Muntean, and D. Hulea, "Bidirectional power flow control in a DC microgrid through a switched-capacitor cell hybrid DC–DC converter," *IEEE Tran. on Ind. Electron.*, vol. 64, no. 4, pp. 3012–3022, 2017.

[8] M. Farrokhabadi, B. V. Solanki, C. A. Canizares, K. Bhattacharya,S. Koenig, P. S. Sauter, T. Leibfried, and S. Hohmann, "Energy storage in microgrids: compensating for generation and demand fluctuations while providing ancillary services," *IEEE Power and Energy Mag.*, vol. 15, no. 5, pp. 81–91, Sept 2017.

[9] M. Kwon and S. Choi, "Control scheme for autonomous and smooth mode switching of bidirectional DC-DC converters in a DC microgrid," *IEEE Trans. on Power Electron.*, vol. 33, no. 8, pp. 7094–7104, Aug 2018.

[10] C. c. Lin, L. s. Yang, and G. W. Wu, "Study of a non-isolated bidirectional DC- DC converter," *IET Power Electron.,* vol. 6, no. 1, pp. 30–37, Jan 2013.

[11] A. A. Khan, Honnyong Cha, and H. F. Ahmed, "A family of high efficiency bidirectional DC-DC converters using switching cell structure," in *Proc. of 2016 IEEE 8th Int. Power Electron. and Motion Control Conf.(IPEMC-ECCE Asia)*, 2016, pp. 1177–1183.

[12] J. M. Guerrero, P. C. Loh, T. Lee, and M. Chandorkar, "Advanced control architectures for intelligent microgrids—part II: power quality, energy storage, and CC/DC microgrids," *IEEE Trans. on Ind. Electron.*, vol. 60, no. 4, pp. 1263–1270, 2013.

[13] M. Forouzesh, Y. P. Siwakoti, S. A. Gorji, F. Blaabjerg, and B. Lehman, "Step-up DC–DC converters: a comprehensive review of voltage-boosting techniques, topologies, and applications," *IEEE Trans. on Power Electron.*, vol. 32, no. 12, pp. 9143–9178, Dec 2017.

[14] X. She, A. Q. Huang, and R. Burgos, "Review of solid-state transformer technologies and their application in power distribution systems," *IEEE J. of Emerging and Select. Topics in Power Electron.*, vol. 1, no. 3, pp. 186–198, Sept 2013.

[15] M. Das and V. Agarwal, "Design and analysis of a high-efficiency

DC–DC converter with soft switching capability for renewable energy applications requiring high voltage gain," *IEEE Trans. on Ind. Electron.*, vol. 63, no. 5, pp. 2936–2944, May 2016.

[16] S. Kouro, J. I. Leon, D. Vinnikov, and L. G. Franquelo, "Grid-connected photovoltaic systems: an overview of recent research and emerging PV converter technology," *IEEE Ind. Electron. Maga*., vol. 9, no. 1, pp. 47–61, March 2015.

[17] D. Han, J. Noppakunkajorn, and B. Sarlioglu, "Comprehensive efficiency, weight, and volume comparison of SiC- and Si-based bidirectional DC–DC converters for hybrid electric vehicles," *IEEE Trans. on Veh. Technol*., vol. 63, no. 7, pp. 3001–3010, Sept 2014.

[18] J. Mill´an, P. Godignon, X. Perpi˜n`a, A. P´erez-Tom´as, and J. Rebollo, "A survey of wide bandgap power semiconductor devices," *IEEE Trans.on Power Electron.*, vol. 29, no. 5, pp. 2155–2163, May 2014.

[19] A. Marzoughi, A. Romero, R. Burgos, and D. Boroyevich, "Comparing the state-of-the-art SiC MOSFETs: test results reveal characteristics of four major manufacturers? 900-v and 1.2-kv SiC devices," *IEEE Power Electron. Mag.*, vol. 4, no. 2, pp. 36–45, June 2017.

[20] A. Anthon, Z. Zhang, M. A. E. Andersen, D. G. Holmes, B. McGrath, and C. A. Teixeira, "The benefits of SiC MOSFETs in a T-Type inverter for grid-tie applications," *IEEE Trans. on Power Electron.*, vol. 32, no. 4, pp. 2808–2821, April 2017.

[21] D. Han, J. Noppakunkajorn, and B. Sarlioglu, "Comprehensive efficiency, weight, and volume comparison of SiC- and Si-based bidirectional DC–DC converters for hybrid electric vehicles," *IEEE Trans. on Veh. Technology*, vol. 63, no. 7, pp. 3001–3010, Sept 2014.

[22] H. A. Mantooth, K. Peng, E. Santi, and J. L. Hudgins, "Modeling of wide bandgap power semiconductor devices–part I," *IEEE Trans. on Electron Devices*, vol. 62, no. 2, pp. 423–433, Feb 2015.

[23] J. C. Balda and A. Mantooth, "Power-semiconductor devices and compo-nents for new power converter developments: a key enabler for ultrahigh efficiency power electronics," *IEEE Power Electron. Mag*., vol. 3, no. 2, pp. 53–56, June 2016.

[24] T. P. Chow, I. Omura, M. Higashiwaki, H. Kawarada, and V. Pala, "smart power devices and ICs using GaAs and wide and extreme bandgap semiconductors," *IEEE Trans. Electron Devices,* vol. 64, no. 3, pp. 856–873, March 2017.

[25] K. Shenai, "Future prospects of widebandgap (WBG) semiconductor power switching devices," *IEEE Trans. on Electron Devices*, vol. 62, no. 2, pp. 248–257, Feb 2015.

[26] S. S. Alharbi, S. S. Alharbi, A. M. S. Al-bayati, and M. Matin, "Design and performance evaluation of a DC-DC buck-boost converter with cascode GaN FET, SiC JFET, and Si IGBT power devices," in *Proc. of 2017 North Amer. Power Symp. (NAPS)*, Sept 2017, pp. 1–6.

[27] K. Shenai and A. Chattopadhyay, "Optimization of high-voltage wide bandgap semiconductor power diodes," *IEEE Trans. on Electron Devices*, vol. 62, no. 2, pp. 359–365, Feb 2015.

[28] T. P. Chow, "Wide bandgap semiconductor power devices for energy efficient systems," in *Proc. of 2015 IEEE 3rd Workshop on Wide Bandgap Power Devices and Applicat. (WiPDA)*, 2015, pp. 402–405.

[29] N. Kaminski, "State of the art and the future of wide band-gap devices," in *Proc. of 2009 13th European Conf. on Power Electron. and Applicat*., Sep. 2009, pp. 1–9.

[30] C. M. DiMarino, R. Burgos, and B. Dushan, "High-temperature silicon carbide: characterization of state-of-the-art silicon carbide power transis-tors," *IEEE Ind. Electron. Mag*., vol. 9, no. 3, pp. 19–30, 2015.

[31] Y. Wang, B. Chen, Y. Hou, Z. Meng, and Y. Yang, "Analysis and design of a 1-MHz bidirectional multi-CLLC resonant DC-DC converter with GaN devices," *IEEE Trans. on Ind. Electron.*, vol. 67, no. 2, pp. 1425–1434, Feb 2020.

[32] K. Shenai, "Wide bandgap (WBG) semiconductor power converters for DC microgrid applications," in *Proc. of 2015 IEEE First Int. Conf. on DC Microgrids (ICDCM)*, June 2015, pp. 263–268.

[33] X. Ding, Y. Zhou, and J. Cheng, "A review of gallium nitride power device and its applications in motor drive," *CES Trans. on Elect. Machines and Syst*., vol. 3, no. 1, pp. 54–64, 2019.

[34] E. A. Jones, F. F. Wang, and D. Costinett, "Review of commercial GaN power devices and GaN-based converter design challenges," *IEEE J. of Emerging and Select. Topics in Power Electron*., vol. 4, no. 3, pp. 707–719, Sep. 2016.

[35] C. D. Santi, M. Meneghini, G. Meneghesso, and E. Zanoni, "Review of dynamic effects and reliability of depletion and enhancement GaN HEMTs for power switching applications," *IET Power Electron.*, vol. 11, no. 4, pp. 668–674, (2018).

[36] F. Xue, R. Yu, and A. Q. Huang, "A 98.3% efficient GaN isolated bidirectional DC–DC converter for DC microgrid energy storage system applications," *IEEE Trans. on Ind. Electron.*, vol. 64, no. 11, pp. 9094–9103, Nov 2017.

[37] F. C. Lee and Q. Li, "High-frequency integrated point-of-load converters: overview," *IEEE Trans. on Power Electron.*, vol. 28, no. 9, pp. 4127–4136, Sep. 2013.

[38] Y. Guan, Y. Wang, D. Xu, and W. Wang, "A 1 MHz half-bridge resonant DC/DC converter based on GaN FETs and planar magnetics," *IEEE Trans. on Power Electron*., vol. 32, no. 4, pp. 2876–2891, April 2017.

[39] W. Qian, X. Zhang, Y. Fu, J. Lu, and H. Bai, "Applying normally-off GaN HEMTs for coreless high-frequency wireless chargers," *CES Trans. on Elect. Machines and Syst*., vol. 1, no. 4, pp. 418–427, December 2017.

[40] E. Gurpinar, Y. Yang, F. Iannuzzo, A. Castellazzi, and F. Blaabjerg, "Reliability-driven assessment of GaN HEMTs and Si IGBTs in 3L-ANPC PV inverters," *IEEE J. of Emerging and Select. Topics in Power Electron*., vol. 4, no. 3, pp. 956–969, Sep. 2016.

[41] A. S. Abdelrahman, Z. Erdem, Y. Attia, and M. Z. Youssef, "Wide bandgap devices in electric vehicle converters: A performance survey," *Canadian J. of Elect. and Comput. Eng*., vol. 41, no. 1, pp. 45–54, winter 2018.

[42] E. Gurpinar and A. Castellazzi, "Single-phase T-type inverter perfor-mance benchmark using Si IGBTss, SiC MOSFETs, and GaN HEMTs," **IEEE Trans.on Power Electron.**, vol. 31, no. 10, pp. 7148–7160, Oct 2016.

[43] R. Yan, J. Xi, and L. He, "A 2–10 MHz GaN HEMTs half-bridge driver with bandgap reference comparator clamping and dual level shifters for automotive applications," *IEEE Trans. on Ind. Electron.*, vol. 67, no. 2, pp. 1446–1454, Feb 2020.

[44] G. Zulauf, S. Park, W. Liang, K. N. Surakitbovorn, and J. Rivas-Davila, "COSS losses in 600 V GaN power semiconductors in soft-switched, high- and very-high-frequency power converters," *IEEE Trans. on Power Electron*., vol. 33, no. 12, pp. 10 748–10 763, Dec 2018.

[45] K. J. Chen, O. H¨aberlen, A. Lidow, C. l. Tsai, T. Ueda, Y. Uemoto, and Y. Wu, "GaN-on-Si power technology: devices and applications," *IEEE Trans. on Electron Devices,* vol. 64, no. 3, pp. 779–795, March 2017.

[46] J. Ren, C. W. Tang, H. Feng, H. Jiang, W. Yang, X. Zhou, K. M. Lau, and J. K. O. Sin, "A novel 700 V monolithically integrated Si-GaN cascoded field effect transistor," *IEEE Electron Device Letters*, vol. 39, no. 3, pp. 394–396, March 2018.

[47] X. Huang, F. C. Lee, Q. Li, and W. Du, "High-frequency high-efficiency GaN-based interleaved CRM bidirectional buck/boost converter with inverse coupled inductor," *IEEE Trans. on Power Electron*., vol. 31, no. 6, pp. 4343–4352, June 2016.

[48] D. Kinzer and S. Oliver, "Monolithic HV GaN power ICs: performance and application," *IEEE Power Electron. Mag.*, vol. 3, no. 3, pp. 14–21, Sept 2016.

[49] J. M. Guerrero, P. C. Loh, T. Lee, and M. Chandorkar, "Advanced control architectures for intelligent microgrids–part II: Power quality, energy storage, and AC/DC microgrids," *IEEE Trans. on Ind. Electron*., vol. 60, no. 4, pp. 1263–1270, 2013.

[50] M. O. Badawy, M. N. Arafat, A. Ahmed, S. Anwar, Y. Sozer, P. Yi, and J. A. De Abreu-Garcia, "Design and implementation of a 75-kW mobile charging system for electric vehicles," *IEEE Trans. on In. Applicat*., vol. 52, no. 1, pp. 369–377, 2016.

[51] S. A. Gorji, H. G. Sahebi, M. Ektesabi, and A. B. Rad, "Topologies and control schemes of bidirectional DC-DC power converters: An overview," *IEEE Access*, vol. 7, pp. 117 997–118 019, 2019.

[52] D. Ji, W. Li, and S. Chowdhury, "A study on the impact of channel mobility on switching performance of vertical GaN MSFETs," *IEEE Trans.on Electron Devices*, vol. 65, no. 10, pp. 4271–4275, 2018.

[53] X. Wang, S. Huang, Y. Zheng, K. Wei, X. Chen, H. Zhang, and X. Liu, "Effect of GaN channel layer thickness on DC and RF performance of GaN HEMTs with composite AlGaN/GaN buffer," *IEEE Trans. on Electron Devices*, vol. 61, no. 5, pp. 1341–1346, May 2014.

[54] Transphorm, "Cascode vs. e-mode," 2018. [Online]. Available: https://www.transphormusa.com/en/document/transphorm-vs-emode.shtml

[55] C. N. M. Ho, H. Breuninger, S. Pettersson, G. Escobar, and F. Canales, "A comparative performance study of an interleaved boost converter using commercial Si and SiC diodes for PV applications," *IEEE Trans.on Power Electron*., vol. 28, no. 1, pp. 289–299, Jan 2013.

[56] A. Le´on-Masich, H. Valderrama-Blavi, J. M. Bosque-Moncus´ı, and L. Mart´ınez-Salamero, "Efficiency comparison between Si and SiC-based implementations in a high gain DC-DC boost converter," *IET Power Electron*., vol. 8, no. 6, pp. 869–878, 2015.

[57] N. Keshmiri, D. Wang, B. Agrawal, R. Hou, and A. Emadi, "Current status and future trends of GaN HEMTs in electrified transportation," *IEEE Access*, vol. 8, pp. 70 553–70 571, 2020.

[58] K. J. Chen, O. H¨aberlen, A. Lidow, C. l. Tsai, T. Ueda, Y. Uemoto, and Y. Wu, "GaN-on-Si power technology: devices and applications," *IEEE Trans. on Electron Devices*, vol. 64, no. 3, pp. 779–795, 2017.

**Salah S. Alharbi** received the B.S. degree in elec-trical engineering from Umm Al Qura University, Mecca, Saudi Arabia, in 2008, and the M.S. degree in electrical engineering from University of Colorado Denver, Denver, CO, USA, in 2015, and the Ph.D. degree in electrical engineering from University of Denver, Denver, CO, USA, in 2020.

He is currently an Assistant Professor of Electrical Engineering in the School of Engineering at Albaha University, Alaqiq, in Saudi Arabia. His research interests include wide bandgap semiconductor devices and power electronic converters as well as inverters for renewable energy applications.

**Mohammad Abdul Matin** received the B.S. (Honors) and M.S. in Applied Physics and Electronics with First Class from the Dhaka University, Bangladesh, and the PhD in Electrical and Electronics Engineering from Nottingham University, United Kingdom, in 1993. He then joined as post-doctoral fellow (94-95) and worked as a Research Engineer (95-98) at the Center for Electro-photonics Materials and Devices, McMaster University, Hamilton, in Canada. He moved to the University of Toronto, in Canada, as a Senior Research Associate (1998-2000).

He is currently a Professor of Electrical and Computer Engineering in the School of Engineering and Computer Science at University of Denver, Denver, CO, in USA. He is a senior Member of IEEE, OSA, SPIE, and member of ASEE and Sigma Xi. His research interests include power electronics and optoelectronic materials, devices and systems, as well as optical and bio-medical signal and image Processing.